Article

Cell Reports

Grxcr1 Promotes Hair Bundle Development by Destabilizing the Physical Interaction between Harmonin and Sans Usher Syndrome Proteins

Graphical Abstract

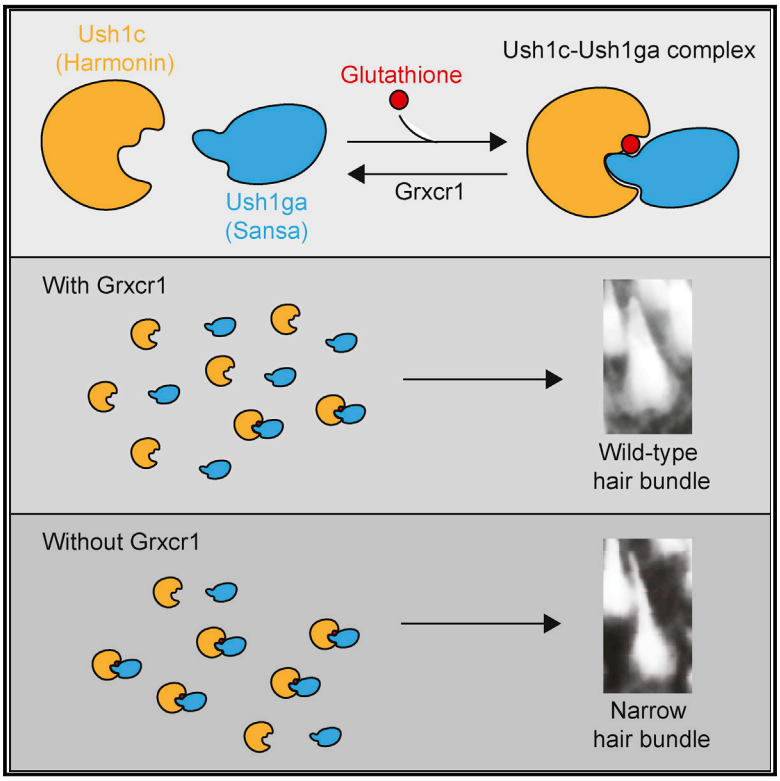

Highlights

- Grxcr1, a deglutathionylating enzyme, promotes hair cell mechanoreceptor development
- *grxcr1*, *ush1c*, and *ush1ga* zebrafish mutants have similar hair bundle defects
- Glutathionylation of Ush1c promotes the interaction between Ush1c and Ush1ga
- Grxcr1 prevents physical interaction between Ush1c and Ush1ga

Authors

Bernardo Blanco-Sánchez, Aurélie Clément, Javier Fierro, Jr., ..., Judy L. Peirce, Philip Washbourne, Monte Westerfield

Correspondence

berde@uoneuro.uoregon.edu (B.B.-S.), monte@uoneuro.uoregon.edu (M.W.)

In Brief

Deafness and vestibular areflexia in Usher syndrome (USH) are due to defective assembly of USH proteins into macromolecular complexes. Blanco-Sánchez et al. show that Grxcr1 negatively regulates the assembly of Ush1c and Ush1ga into complexes and that its activity is essential for correct mechanoreceptor morphology.

Blanco-Sánchez et al., 2018, Cell Reports *25*, 1281–1291
October 30, 2018 © 2018 The Author(s).
https://doi.org/10.1016/j.celrep.2018.10.005

CellPress

Cell Reports
Article

OPEN ACCESS
CellPress

Grxcr1 Promotes Hair Bundle Development by Destabilizing the Physical Interaction between Harmonin and Sans Usher Syndrome Proteins

Bernardo Blanco-Sánchez,[1,3,4,5,*] Aurélie Clément,[1,3] Javier Fierro, Jr.,[1] Sarah Stednitz,[1] Jennifer B. Phillips,[1] Jeremy Wegner,[1] Jennifer M. Panlilio,[2] Judy L. Peirce,[1] Philip Washbourne,[1] and Monte Westerfield[1,*]
[1]Institute of Neuroscience, University of Oregon, Eugene, OR 97403, USA
[2]Woods Hole Oceanographic Institution, Woods Hole, MA 02543, USA
[3]These authors contributed equally
[4]Present address: Institut Imagine, Université Paris Descartes-Sorbonne Paris Cité, Paris 75015, France
[5]Lead Contact
*Correspondence: berde@uoneuro.uoregon.edu (B.B.-S.), monte@uoneuro.uoregon.edu (M.W.)
https://doi.org/10.1016/j.celrep.2018.10.005

SUMMARY

Morphogenesis and mechanoelectrical transduction of the hair cell mechanoreceptor depend on the correct assembly of Usher syndrome (USH) proteins into highly organized macromolecular complexes. Defects in these proteins lead to deafness and vestibular areflexia in USH patients. Mutations in a non-USH protein, glutaredoxin domain-containing cysteine-rich 1 (*GRXCR1*), cause non-syndromic sensorineural deafness. To understand the deglutathionylating enzyme function of GRXCR1 in deafness, we generated two *grxcr1* zebrafish mutant alleles. We found that hair bundles are thinner in homozygous *grxcr1* mutants, similar to the USH1 mutants *ush1c* (Harmonin) and *ush1ga* (Sans). *In vitro* assays showed that glutathionylation promotes the interaction between Ush1c and Ush1ga and that Grxcr1 regulates mechanoreceptor development by preventing physical interaction between these proteins without affecting the assembly of another USH1 protein complex, the Ush1c-Cadherin23-Myosin7aa tripartite complex. By elucidating the molecular mechanism through which Grxcr1 functions, we also identify a mechanism that dynamically regulates the formation of Usher protein complexes.

INTRODUCTION

The hair cells of the inner ear are the sensory cells that mediate hearing and balance. They sense mechanical stimuli induced by sound waves or movement via their mechanoreceptor, an apical organelle bathed in the endolymph. This specialized organelle is composed of a single kinocilium and interconnected actin-rich stereocilia arranged in a staircase pattern that, together, form the hair bundle (Tilney and DeRosier, 1986; Tilney et al., 1986). The mechanoreceptor acts as an antenna, converting mechanical forces into ionic currents that result in signaling to the brain. This process is known as mechanoelectrical transduction (MET). Defects in the morphology or polarity of the mechanoreceptor can affect hair cell function. Thus, the morphogenesis, development, and structural integrity of the mechanoreceptor are tightly regulated. Numerous proteins, including actin-bundling proteins and adhesion molecules, participate in these processes (Barr-Gillespie, 2015; Dror and Avraham, 2009; Lu and Sipe, 2016; McGrath et al., 2017; Petit and Richardson, 2009), although the fine regulation of each process at the molecular level is still understudied.

Glutathionylation is a reversible posttranslational modification of cysteine residues that can alter enzyme activity, protein stability, DNA binding, actin polymerization, and protein distribution. Defects in glutathionylation are linked to many diseases, including cancer (Allocati et al., 2018; Board and Menon, 2016; Johnson et al., 2015; Matsui et al., 2017; Pastore and Piemonte, 2012). Glutaredoxin domain-containing cysteine-rich 1 (GRXCR1) is an enzyme that removes glutathione groups from proteins. Mutations in *GRXCR1* are associated with nonsyndromic hearing loss *DFNB25* (Odeh et al., 2010; Schraders et al., 2010). Patients with mutations in *GRXCR1* present with phenotypic variation, from congenital severe or profound deafness to early-onset mild to moderate hearing loss (Mori et al., 2015; Odeh et al., 2010; Schraders et al., 2010). Some patients report vestibular dysfunction or dizziness. Mice homozygous mutant for *Grxcr1* have profound deafness and abnormal vestibular function (Beyer et al., 2000; Erven et al., 2002). Ultrastructural analysis of the cochlear and vestibular mechanoreceptors showed that *Grxcr1* mutant mice have morphological defects in their stereocilia. In the *Grxcr1* mutant organ of Corti and vestibular system, the staircase arrangement of stereocilia is present at birth but becomes progressively disorganized during subsequent development (Beyer et al., 2000; Erven et al., 2002). In general, stereocilia fail to widen and appear thinner (Erven et al., 2002). These phenotypes are indicative of defects in stereocilium growth, a three-step process characterized by stereocilium elongation, elongation arrest and widening, followed by reinitiation of elongation (Cotanche, 1987). Grxcr1 localizes in the stereocilia of inner ear hair cells (Odeh et al., 2010), but its role in hair bundle development is unknown.

This is an open access article under the CC BY-NC-ND license (http://creativecommons.org/licenses/by-nc-nd/4.0/).

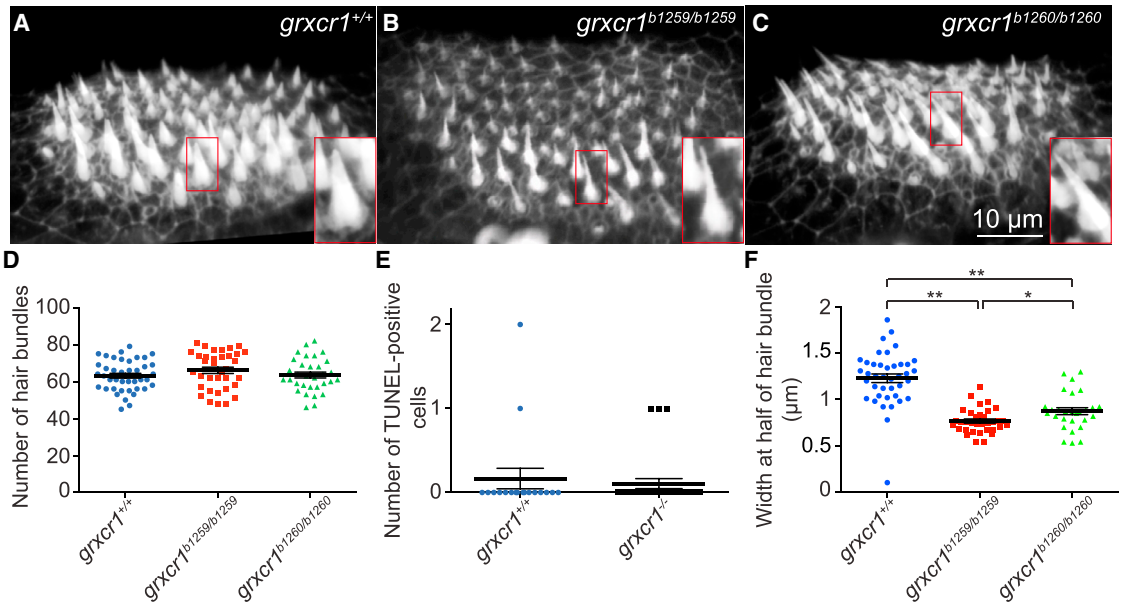

Figure 1. Grxcr1 Is Required for Stereocilium Widening in the Anterior Macula

(A–C) Phalloidin staining of the whole anterior macula in *grxcr1*$^{+/+}$ (A), *grxcr1*$^{b1259/b1259}$ (B), and *grxcr1*$^{b1260/b1260}$ mutant larvae (C).

(D) Average number of hair bundles in *grxcr1*$^{+/+}$ (n = 41 larvae), *grxcr1*$^{b1259/b1259}$ (n = 35 larvae), and *grxcr1*$^{b1260/b1260}$ mutant larvae (n = 32 larvae).

(E) Number of TUNEL-positive cells in *grxcr1*$^{+/+}$ (n = 18 larvae) and *grxcr1*$^{-/-}$ mutant larvae (n = 28 larvae).

(F) Average hair bundle width at half their height in *grxcr1*$^{+/+}$ (n = 40 larvae), *grxcr1*$^{b1259/b1259}$ (n = 34 larvae), and *grxcr1*$^{b1260/b1260}$ mutant larvae (n = 36 larvae).

Data are represented as mean ± SEM. *p < 0.05, **p < 0.01; 5 dpf.

Stereocilium growth depends on the proper assembly of the tip link, a complex of Usher syndrome type 1 (USH1) proteins. Disorganization of stereocilia in *Grxcr1* mutant mice is reminiscent of that observed in *USH1* mutant mice and zebrafish (Blanco-Sánchez et al., 2014; Ernest et al., 2000; Johnson et al., 2003; Lefèvre et al., 2008; Phillips et al., 2011; Seiler et al., 2005; Söllner et al., 2004). In humans, mutations in *USH1* genes prevent tip link assembly and lead to non-syndromic deafness or Usher syndrome (USH), a condition characterized by congenital deafness, vestibular areflexia, and progressive retinal degeneration (Mathur and Yang, 2015). Harmonin, encoded by *USH1C*, and Sans, encoded by *USH1G*, are two USH1 scaffold proteins that form complexes with other Usher proteins (Mathur and Yang, 2015). Because glutathionylation can affect protein binding (Wang et al., 2018), we hypothesized that Grxcr1 regulates the assembly of USH1 protein complexes. To test this, we created two zebrafish *grxcr1* mutants and analyzed USH1 protein interactions. We found that Ush1c (Harmonin) and Ush1ga (one of the two zebrafish Sans proteins) are glutathionylated or bound to a glutathionylated protein and that removal of the glutathione by Grxcr1 promotes interaction of Ush1c with Ush1ga.

RESULTS

Grxcr1 Is Required for Stereocilium Elongation

To understand the role of Grxcr1 in hair cells, we first verified that *grxcr1* is expressed in developing hair cells. RT-PCR analysis showed that *grxcr1* is maternally deposited and then expressed until at least early larval stages, when hair cells become functional in zebrafish (Figure S1A). Using an RNA probe spanning the four coding exons of *grxcr1*, we found, by *in situ* hybridization, that this gene is expressed specifically in the brain, eyes, and hair cells of the inner ear and neuromasts 5 days postfertilization (dpf; Figures S1B and S1C).

To study Grxcr1 function, we generated two independent *grxcr1* mutant alleles that delete the glutaredoxin domain. Mutations in the *grxcr1*^{b1259} and *grxcr1*^{b1260} alleles delete 19 bp in exon 1 and 8 bp in exon 2, respectively (Figures S2A and S2B). In each allele, deletions lead to a shift of the open reading frame that introduces either 64 amino acids (*grxcr1*^{b1259}) or 1 (*grxcr1*^{b1260}) amino acid, followed by an early stop codon. The mutant Grxcr1^{b1259} protein lacks the entire glutaredoxin domain, whereas Grxcr1^{b1260} lacks about a third of the enzymatic domain (Figure S2C).

We first analyzed the structure of the anterior macula at 5 dpf. We found that the number of hair bundles and hair cells was similar in *grxcr1* mutant and wild-type (WT) sibling larvae (Figures 1A–1D and S3A). Consistent with this, we found no change in cell death, as indicated by terminal deoxynucleotidyl transferase 2'-deoxyuridine, 5'-triphosphate (dUTP) nick end labeling (TUNEL; Figure 1E).

Analysis of mechanoreceptors in *grxcr1*$^{-/-}$ mutants revealed defects in hair bundle morphology at 5 dpf (Figures 1B and 1C). Normally, at this stage of development, hair bundles appear conical because of the staircase organization of the stereocilia labeled by phalloidin (Figure 1A). To quantify morphological changes, we measured the hair bundle height, width at the

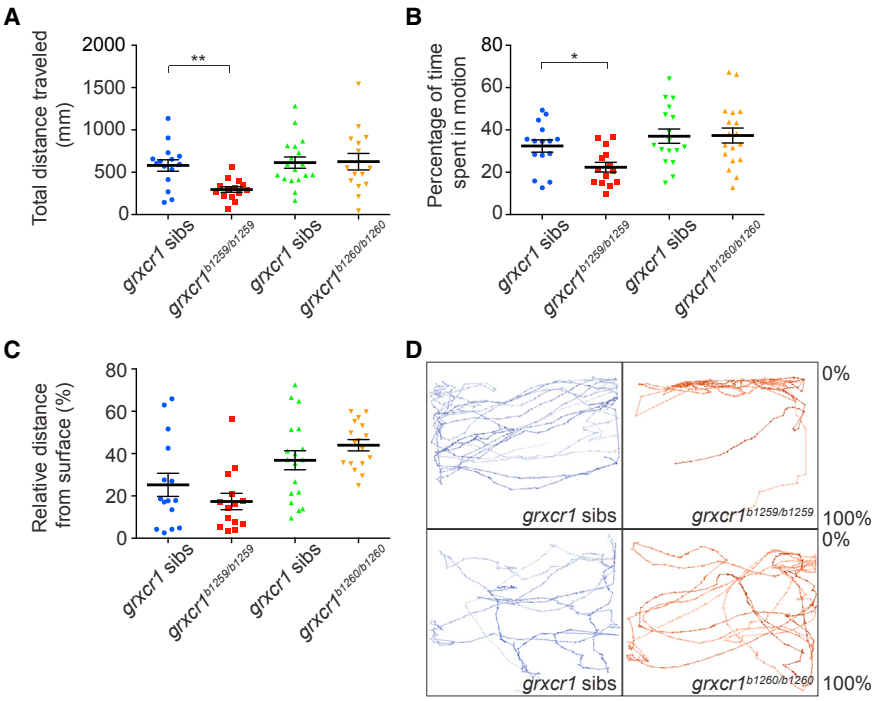

Figure 2. Locomotor Activity Is Decreased in *grxcr1*$^{-/-}$ Mutants

(A) Total distance traveled by *grxcr1*^{b1259} siblings (n = 15), *grxcr1*$^{b1259/b1259}$ mutant larvae (n = 14), *grxcr1*^{b1260} siblings (n = 18), and *grxcr1*$^{b1260/b1260}$ mutant larvae (n = 17) during a period of 5 min.

(B) Percentage of time *grxcr1*^{b1259} siblings (n = 15), *grxcr1*$^{b1259/b1259}$ mutant larvae (n = 14), *grxcr1*^{b1260} siblings (n = 18), and *grxcr1*$^{b1260/b1260}$ mutant larvae (n = 15) spent in motion during a period of 5 min.

(C) Average relative distance, in percent, of *grxcr1*^{b1259} siblings (n = 15), *grxcr1*$^{b1259/b1259}$ mutant larvae (n = 14), *grxcr1*^{b1260} siblings (n = 18), and *grxcr1*$^{b1260/b1260}$ mutant larvae (n = 17) from the water surface. 0% corresponds to the water surface, and 100% corresponds to the bottom of the water column.

(D) Representative traces of the routes taken by *grxcr1* siblings and *grxcr1*$^{b1259/b1259}$ mutant larvae during a 5-min period.

Data are represented as mean ± SEM. *p < 0.05, **p < 0.01; 5 dpf.

base, and width at half the height of the tallest hair bundles in the extra-striolar region of the anterior macula. In *grxcr1*$^{+/+}$ larvae, hair bundles had an average height of 4.9 μm, an average base width of 2 μm, and an average mid-height width of 1.2 μm (Figures 1F, S3B, and S3C). In *grxcr1*$^{-/-}$ mutants, hair bundles were longer than in *grxcr1*$^{+/+}$ larvae (8% longer in *grxcr1*$^{b1259/b1259}$ and 15% longer in *grxcr1*$^{b1260/b1260}$) and had a slightly different base width (4% narrower in *grxcr1*$^{b1259/b1259}$ and 11% wider in *grxcr1*$^{b1260/b1260}$) (Figures S3B and S3C). However, the most striking phenotype was a reduced width at mid-height of the hair bundle ranging from 37% in *grxcr1*$^{b1259/b1259}$ to 29% in *grxcr1*$^{b1260/b1260}$ (Figure 1F). The slender hair bundle phenotype is significantly more severe in *grxcr1*$^{b1259/b1259}$ mutants than in *grxcr1*$^{b1260/b1260}$ mutants (Figures 1F, S3B and S3C). In contrast to the mutant Grxcr1^{b1259} protein that lacks the whole glutaredoxin domain, the mutant Grxcr1^{b1260} protein misses only about a third of the domain. It is thus possible that the mutant Grxcr1^{b1260} protein retains some residual activity. This result suggested a defect of stereocilium growth and was consistent with previous observations in *Grxcr1* mouse mutants (Erven et al., 2002). Complementation tests between the two *grxcr1* alleles failed to rescue the observed hair bundle defects (Figures S3D–S3H), demonstrating that the thinner and longer hair bundle phenotype is specifically due to loss of Grxcr1 function.

grxcr1 Mutants Have Decreased Locomotor Activity

Hair cell defects in USH1 and some other heritable diseases of deafness result in vestibular as well as hearing defects. To characterize the functional consequences of *grxcr1* mutation on balance, we analyzed the behavior of *grxcr1*$^{-/-}$ mutant larvae and their siblings at 5 dpf. We first measured the total distance traveled by the larvae over a period of 5 min (Figure 2A) as well as the time spent in motion during that period (Figure 2B). The two groups of *grxcr1* sibling larvae swam an average of 580 and 614 mm and were in motion 32% and 37% of the time, respectively. In contrast, *grxcr1*$^{b1259/b1259}$ mutants swam about 297 mm, 51% of the distance traveled by their siblings, and were in motion 22% of the time, a third less than their siblings. These results indicate a significant decrease in locomotion in *grxcr1*$^{b1259/b1259}$ mutants. In contrast, we found that *grxcr1*$^{b1260/b1260}$ mutants swam about 625 mm and were in motion 37% of the time, comparable with their siblings. We then examined the routes followed by each larva to assay spatial exploratory activity. We found that, unlike their siblings, *grxcr1*$^{b1259/b1259}$ mutants spend more time close to the surface of the water than exploring their environment, whereas *grxcr1*$^{b1260/b1260}$ mutants spend more time exploring their environment, similar to their siblings (Figures 2C and 2D). The differences in the hair cell phenotypes between the *grxcr1*$^{b1259/b1259}$ and *grxcr1*$^{b1260/b1260}$ mutants (Figure 1) thus correlate with differences in locomotion defects (Figure 2). The significant decreases in locomotor activity in the more severely affected *grxcr1*$^{b1259/b1259}$ mutants could correlate with the vestibular dysfunction and dizziness reported by some patients (Mori et al., 2015; Schraders et al., 2010).

We also assayed other aspects of hair cell function and found that *grxcr1*$^{-/-}$ mutants performed normally in the startle response test at 5 dpf (Figure S4A). In addition, incorporation of FM1-43 into the hair bundles of hair cells from the anterior macula and the neuromasts was normal (Figures S4B–S4E). These results suggested that, unlike in USH1 mutants, there were no mechanosensory defects in *grxcr1*$^{-/-}$ mutants at this stage of development. Homozygous *grxcr1* mutants are viable. We thus tested behavior in adults using the potentiated

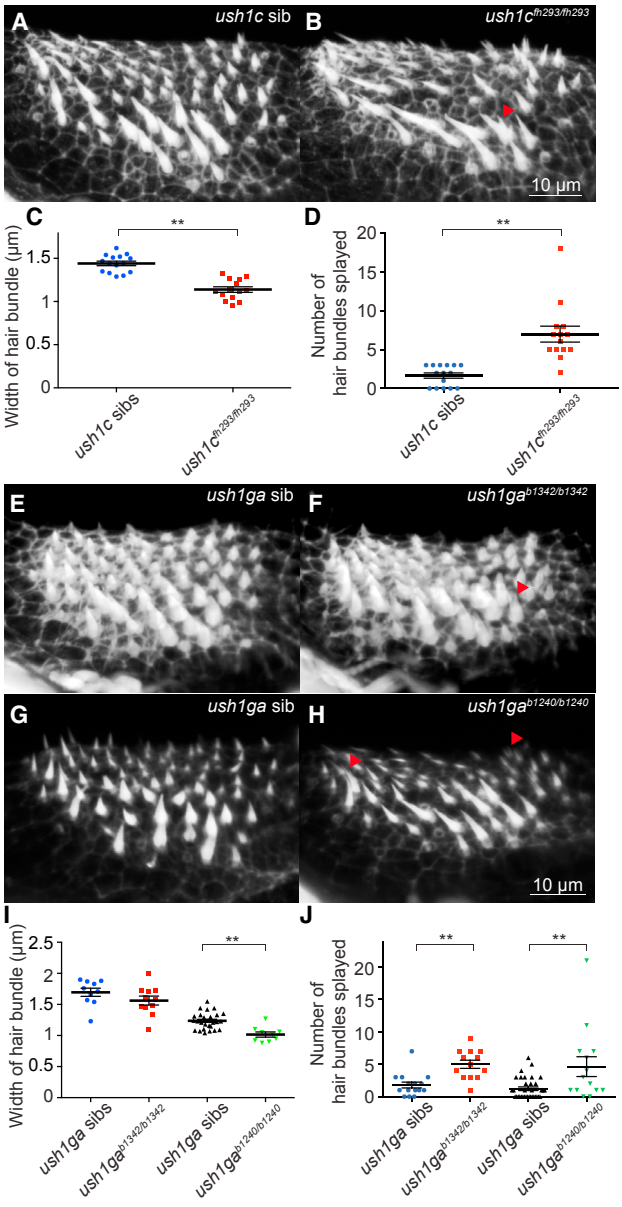

Figure 3. *ush1c*$^{-/-}$ and *ush1ga*$^{-/-}$ Mutants Have Dysmorphic Hair Bundles

(A and B) Phalloidin staining of the anterior macula in *ush1c* siblings (A) and *ush1c*$^{fh293/fh293}$ mutant larvae (B). The red arrowhead points to splayed hair bundles.

(C) Average width of hair bundles at half their height in *ush1c*^{fh293} siblings (n = 15 larvae) and *ush1c*$^{fh293/fh293}$ (n = 14 larvae).

(D) Number of hair bundles splayed in *ush1c*^{fh293} siblings (n = 15 larvae) and *ush1c*$^{fh293/fh293}$ (n = 14 larvae).

(E–H) Phalloidin staining of the anterior macula at in *ush1ga* siblings (E and G), *ush1ga*$^{b1342/b1342}$ (F), and *ush1ga*$^{b1240/b1240}$ mutant larvae (H).

(I) Average hair bundle width at half their height in *ush1ga*^{b1342} siblings (n = 10 larvae), *ush1ga*$^{b1342/b1342}$ (n = 11 larvae), *ush1ga*^{b1240} siblings (n = 28 larvae), and *ush1ga*$^{b1240/b1240}$ mutant larvae (n = 9 larvae).

(J) Number of hair bundles splayed in *ush1ga*^{b1342} siblings (n = 15 larvae), *ush1ga*$^{b1342/b1342}$ (n = 13 larvae), *ush1ga*^{b1240} siblings (n = 35 larvae), and *ush1ga*$^{b1240/b1240}$ mutant larvae (n = 14 larvae).

Data are represented as mean ± SEM. **p < 0.01; 5 dpf.

dorsal light reflex (Nicolson et al., 1998) and found a normal response. Together, our results indicate that the tip links are functional and that MET does not depend upon Grxcr1 activity.

The Hair Bundle Morphology of *grxcr1* Mutants Is Reminiscent of *ush1c* and *ush1ga* Mutants

In zebrafish, mutations in the USH1 genes *cadherin 23* (*cdh23*), *protocadherin 15a*, and *myosin 7aa* (*myo7aa*) lead to severe structural defects of the hair bundles with splayed stereocilia (Blanco-Sánchez et al., 2014; Ernest et al., 2000; Seiler et al., 2005; Söllner et al., 2004). However, we previously showed that *ush1c* mutants have a milder hair bundle phenotype (Blanco-Sánchez et al., 2014; Phillips et al., 2011), and zebrafish *ush1g* mutants have not been described.

As in *grxcr1* mutants, we measured the hair bundle height and the width at half height in *ush1c*$^{fh293/fh293}$ mutants and siblings. We found that hair bundles were significantly longer (9%), thinner (21%), and more frequently splayed (4 times) in *ush1c* mutants than in their siblings (Figures 3A–3D and S3I).

Zebrafish have two *USH1G* orthologs, *ush1ga* and *ush1gb*. To compare *grxcr1* and *ush1g* mutant phenotypes, we generated two independent mutant alleles of *ush1ga*. The *ush1ga*^{b1342} allele contains a 10-bp deletion in exon 2, and the *ush1ga*^{b1240} allele has a 13-bp deletion in exon 1 (Figures S5A and S5B). These deletions lead to frameshifts that introduce 6 (*ush1ga*^{b1342}) or 5 (*ush1ga*^{b1240}) amino acids, followed by early stop codons. The mutant Ush1ga^{b1342} protein lacks the sterile alpha motif (SAM) domain, whereas Ush1ga^{b1240} lacks both the ankyrin repeat (ANK) and SAM domains (Figure S5C).

Examination of mechanoreceptors of the anterior macula in *ush1g* mutants revealed defects in hair bundle morphology. We found that hair bundles were 10% longer and 8% narrower at half height in *ush1ga*$^{b1342/b1342}$ and 12% longer and 18% narrower at half height in *ush1ga*$^{b1240/b1240}$ mutants (Figures 3E–3I and S3J). In addition, there were about 3 times more splayed hair bundles in the *ush1ga*$^{b1342/b1342}$ mutants and 4 times more in *ush1ga*$^{b1240/b1240}$ than in WT siblings (Figure 3J). Analysis of the anterior macula also revealed significant decreases in the number of hair cells and hair bundles in *ush1ga*$^{b1342/b1342}$ but no significant differences in *ush1ga*$^{b1240/b1240}$ (Figures S3K and S3L). This latter result could be due to the presence of a second transcript variant of *ush1ga*. Supporting this, Ensembl (Ensembl Release 92) predicts a second transcript with a start codon in exon 2 (Zerbino et al., 2018), downstream of the *ush1ga*$^{b1240/b1240}$ frameshift in exon 1.

Together, our data show that *grxcr1*, *ush1c*, and *ush1ga* zebrafish mutants have very similar phenotypes with significantly thinner, fewer hair bundles and splayed stereocilia. These phenotypes differ from those found in the USH1 *cdh23*, *pcdh15a*, and *myo7aa* mutants and suggest that Grxcr1, Ush1c, and Ush1ga might act together to regulate hair bundle morphogenesis.

Ush1c Is Glutathionylated

Because of the deglutathionylation activity of Grxcr1 and the overlap in phenotypes of the three types of mutants, we

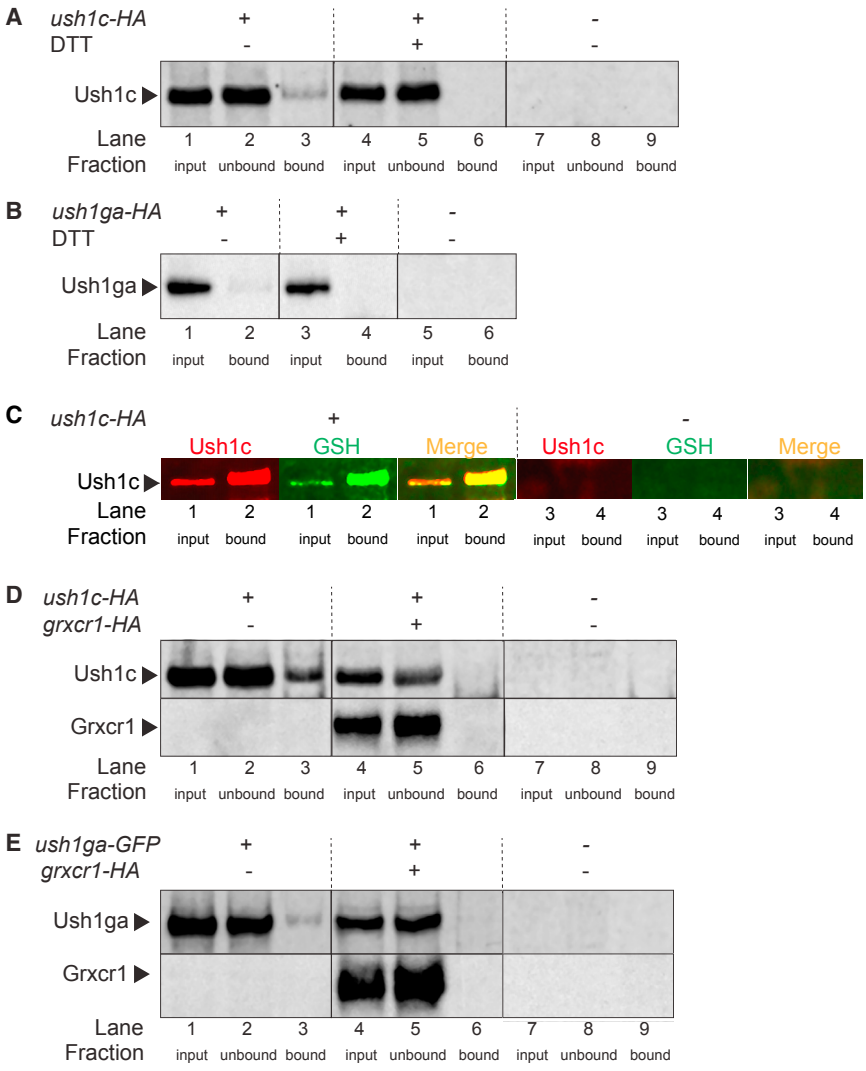

Figure 4. Glutathionylated Ush1c and Ush1ga Are Substrates of Grxcr1

(A) MDCK cells were transfected with *ush1c-HA* (+) or not (–) and treated with DTT (+) or not (–).

(B) MDCK cells were transfected with *ush1ga-HA* (+) or not (–) and treated with DTT (+) or not (–).

(C) MDCK cells were transfected with *ush1c-HA* (+) or not (–).

(D) MDCK cells were transfected with *ush1c-HA* (+) and *grxcr1-HA* (+) or not (–).

(E) MDCK cells were transfected with *ush1ga-GFP* (+) and *grxcr1-HA* (+) or not (–).

For the experiments in (A), (B), (D), and (E), extracted proteins were immunoprecipitated using an anti-GSH antibody. For the experiments in (C), extracted proteins were immunoprecipitated using an anti-Ush1c antibody.

examined whether Ush1c and Ush1ga are glutathionylated. Each contains cysteine residues, one in Ush1c and seven in Ush1ga, that are potential sites for glutathionylation. We transfected Madin-Darby canine kidney (MDCK) cells with a vector encoding hemagglutinin (HA)-tagged Ush1c or HA-tagged Ush1ga. Cell lysates were immunoprecipitated using an antibody against glutathione (GSH) and then analyzed by immunoblot with Ush1c or HA antibodies. Under nonreducing conditions, Ush1c (Figure 4A, lane 3) and a small amount of Ush1ga (Figure 4B, lane 2) were detected in the bound fraction. This result indicated that Ush1c and Ush1ga are either glutathionylated or co-precipitate with a glutathionylated protein.

When DTT, an agent that reduces disulfide bridges in proteins, was added to the cell medium for 1 hr and removed prior to immunoprecipitation, neither Ush1c nor Ush1ga were detected in the bound fraction (Figure 4A, lane 6; Figure 4B, lane 4). This result indicated that the immunoprecipitation of Ush1c and Ush1ga under nonreducing conditions depends on the presence of glutathionylated residues and that pull-down conditions were stringent and specific to glutathionylated proteins (Shao et al., 2014). In addition, in cells not expressing HA-tagged Ush1c or HA-tagged Ush1ga, Ush1c and Ush1ga were not detected in the input, unbound, or bound fractions (Figure 4A, lanes 7–9; Figure 4B, lanes 5 and 6), indicating that there was no background expression of the untagged proteins.

To learn whether Ush1c is glutathionylated directly, we transfected MDCK cells with a vector encoding HA-tagged Ush1c. Cell lysates were immunoprecipitated using an antibody against Ush1c and then analyzed by immunoblot with Ush1c and GSH antibodies. The band recognized by the Ush1c antibody was also detected by the GSH antibody (Figure 4C, lanes 1 and 2). No bands were observed when the vector encoding HA-tagged Ush1c was not transfected (Figure 4C, lanes 3 and 4). This result indicates that Ush1c is glutathionylated.

USH Complex Proteins Are Substrates of Grxcr1

To test whether Grxcr1 deglutathionylates Ush1c, we transfected MDCK cells with a vector encoding HA-tagged Ush1c or with vectors encoding both HA-tagged Ush1c and HA-tagged Grxcr1. After immunoprecipitation with an antibody against GSH and immunoblot analysis with an antibody against Ush1c, Ush1c was detected in the bound fraction only when cells were transfected with HA-tagged Ush1c (Figure 4D, lane 3) but not when cells were co-transfected with both HA-tagged Ush1c and HA-tagged Grxcr1 (Figure 4D, lane 6). Detection of Ush1c and Grxcr1 in the input and unbound fractions (Figure 4D, lanes 4 and 5, respectively) showed that co-transfected cells expressed both proteins and that failure to detect Ush1c in the bound fraction is due to deglutathionylation by Grxcr1.

Similar experiments were done using GFP-tagged Ush1ga. After immunoprecipitation with an antibody against GSH and

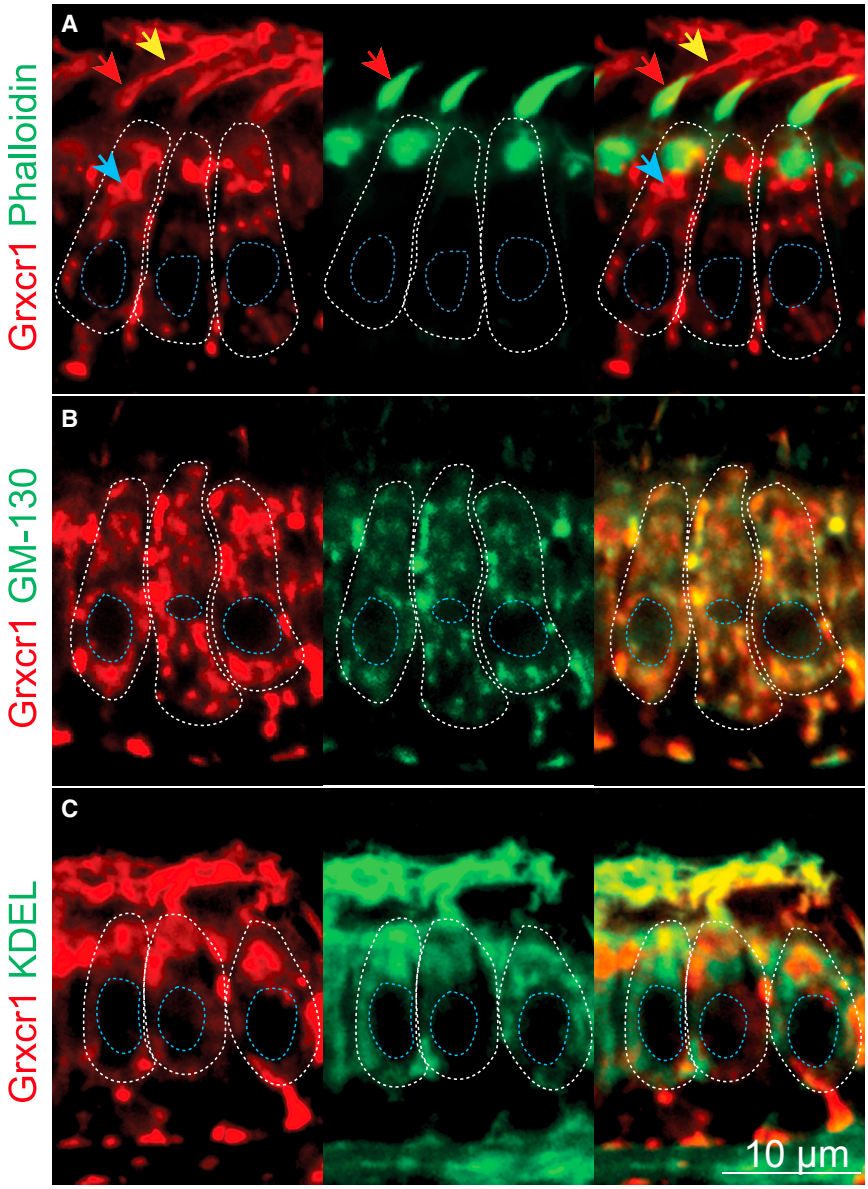

Figure 5. Grxcr1 Localizes in the Golgi Apparatus and ERGIC of the Hair Cells

(A–C) Confocal sections of the anterior macula. Shown are partial colocalization of Grxcr1 (red) and phalloidin (A), GM130 (B), or KDEL (green, C). Individual hair cells are outlined in white. Blue, red, and yellow arrows show Grxcr1 localization in the cell body, hair bundles, and kinocilia, respectively. The confocal sections were selected based on the localization of the organelles of interest (hair bundles, Golgi, and ER), hence the differences in Grxcr1 localization. Nuclei are outlined in blue; 5 dpf.

immunoblot analysis with an antibody against GFP, Ush1ga was detected in the bound fraction only when cells were transfected with GFP-tagged Ush1ga (Figure 4E, lane 3) but not when cells were co-transfected with both GFP-tagged Ush1ga and HA-tagged Grxcr1 (Figure 4E, lane 6).

Together, these data indicate that glutathionylated Ush1c is a substrate of Grxcr1 and that glutathionylated Ush1ga or a glutathionylated protein to which Ush1ga binds (possibly Ush1c) are substrates of Grxcr1.

Grxcr1 Activity May Affect Protein Trafficking

To understand where Grxcr1 acts in hair cells, we used an antibody specific to Grxcr1 (Figures S6A–S6D). We found Grxcr1 associated with both the stereocilia and kinocilium of the mechanoreceptor (Figure 5A, red and yellow arrows, respectively). This result is consistent with the previously described localization of Grxcr1 in the mouse (Odeh et al., 2010). In addition, we also observed Grxcr1 protein in the hair cell body (Figure 5A, blue arrow). Co-immunolabeling with the subcellular compartment markers GM130 and KDEL (amino acid sequence composed of lysine, aspartic acid, glutamic acid, and leucine) showed that Grxcr1 is mostly enriched in the *cis*-Golgi and sub-domains of the endoplasmic reticulum (ER)-Golgi intermediate compartment (ERGIC) (Figure 5B) and, to some extent, in the ER (Figure 5C). Interestingly, we also observed KDEL in the kinocilia and hair bundles. This result was reproduced in larvae expressing the transgene *Tg[myo6b:kdel-crimson]*^{b1319}, which allows visualization of the ER in hair cells (Figure S6E) and provides further support that the KDEL antibody is specific. These results demonstrate that Grxcr1 is localized in the subcellular region, where, as we showed previously, the USH1 proteins Ush1c, Cdh23, and Myo7aa preassemble into a complex that is required for proper intracellular trafficking (Blanco-Sánchez et al., 2014).

Because Grxcr1 localizes to the *cis*-Golgi (Figure 5B), we used GM130 to analyze the Golgi structure. We found that the integrity of the Golgi was abnormal in *grxcr1*$^{-/-}$ mutants (Figures 6A–6C). GM130 labeling was 19% greater in mutants than in the WT. Within the Golgi apparatus, proteins are modified and packed into vesicles before they are transported to their final destinations. The abnormal appearance of the Golgi suggested that Grxcr1 functions in the Golgi apparatus and that loss of Grxcr1 activity may affect protein trafficking.

Grxcr1 Prevents the Physical Interaction between Ush1c and Ush1g

To examine whether Grxcr1 may affect protein trafficking, we investigated the subcellular localization of Ush1c and Ush1ga in the cell bodies of anterior macula hair cells. We found that

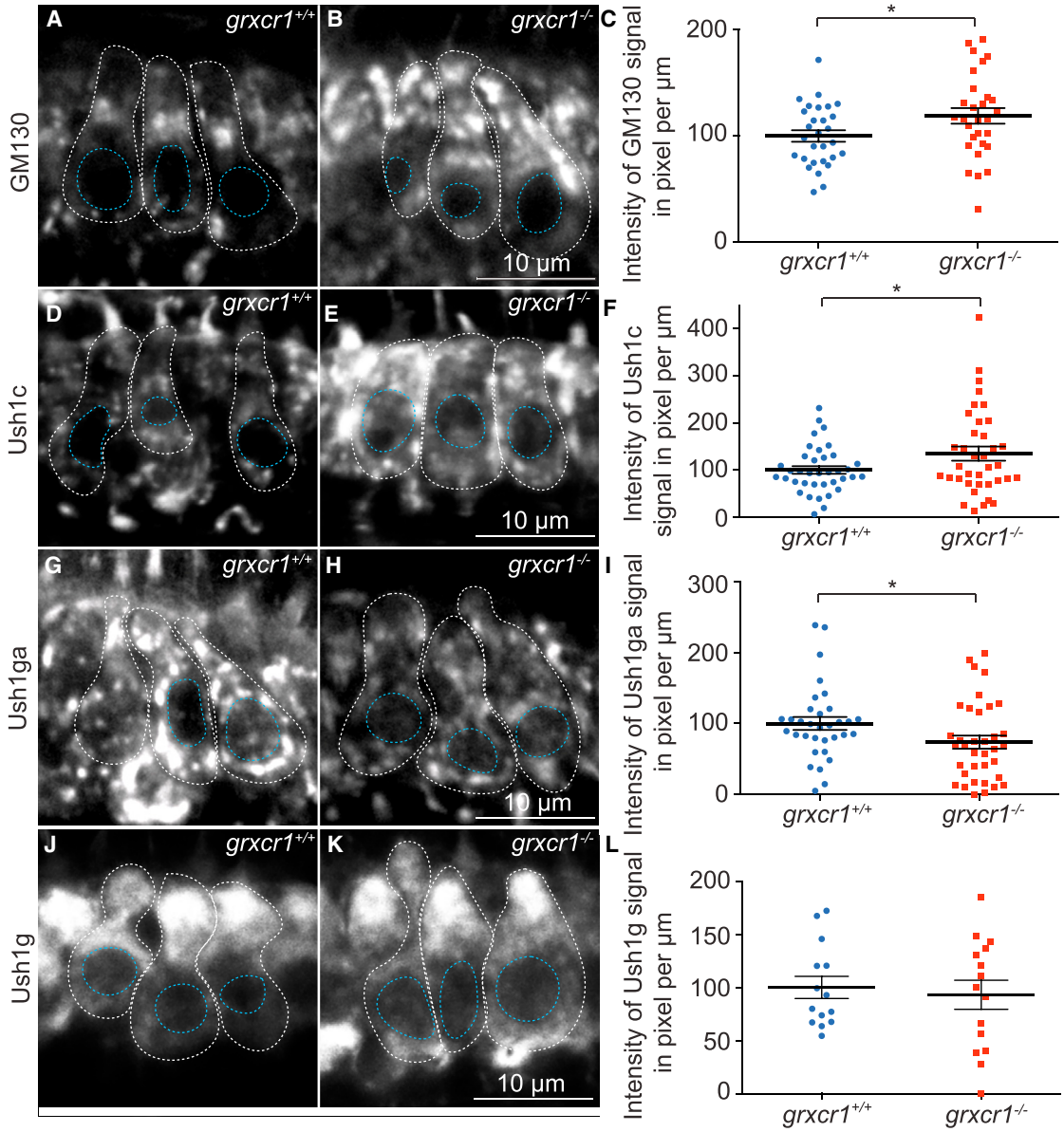

Figure 6. The Integrity of the *cis*-Golgi and Abundance of Ush1c and Ush1ga Are Affected in *grxcr1*$^{-/-}$ Mutants

(A and B) Immunolabeling of GM130 in the anterior maculae of *grxcr1*$^{+/+}$ (A) and *grxcr1*$^{-/-}$ (B).

(C) Quantification of GM130 signal intensity in *grxcr1*$^{+/+}$ (n = 29 larvae) and *grxcr1*$^{-/-}$ (n = 29 larvae) anterior maculae.

(D and E) Immunolabeling of Ush1c in the anterior maculae of *grxcr1*$^{+/+}$ (D) and *grxcr1*$^{-/-}$ larvae (E).

(F) Quantification of Ush1c signal intensity in the anterior macula of *grxcr1*$^{+/+}$ (n = 37 larvae) and *grxcr1*$^{-/-}$ larvae (n = 37 larvae).

(G and H) Immunolabeling of Ush1ga in the anterior maculae of *grxcr1*$^{+/+}$ (G) and *grxcr1*$^{-/-}$ larvae (H).

(I) Quantification of Ush1ga signal intensity in *grxcr1*$^{+/+}$ (n = 33 larvae) and *grxcr1*$^{-/-}$ larvae (n = 36 larvae).

(J and K) Immunolabeling of Ush1g in the anterior maculae of *grxcr1*$^{+/+}$ (J) and *grxcr1*$^{-/-}$ larvae (K).

(L) Quantification of Ush1g signal intensity in *grxcr1*$^{+/+}$ (n = 14 larvae) and *grxcr1*$^{-/-}$ larvae (n = 15 larvae).

Data were normalized to *grxcr1*$^{+/+}$ and are represented as mean ± SEM. *p < 0.05; 5 dpf.

the intensity of the Ush1c signal was increased by 35% in *grxcr1*$^{-/-}$ mutants (Figures 6D and 6F), suggesting an accumulation of Ush1c in the cell body. Using an antibody that recognizes zebrafish Ush1ga but not zebrafish Ush1gb (Figures S6F–S6H), we found that the level of Ush1ga signal was reduced by 26% in *grxcr1*$^{-/-}$ mutants compared with *grxcr1*$^{+/+}$ (Figures 6G–6I). Because the epitope recognized by the Ush1ga antibody is located in the SAM domain, known to interact with Ush1c (Figure S6F; Yan et al., 2010), we examined whether the decrease in the Ush1ga signal was due to the epitope not being accessible. For this, we used a commercially available antibody against human USH1G that targets an

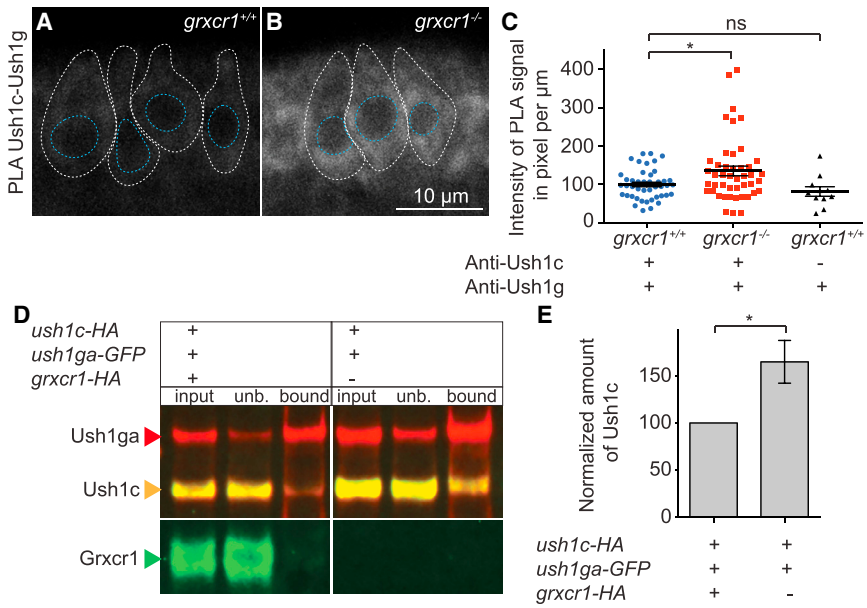

Figure 7. Grxcr1 Destabilizes Ush1c-Ush1ga Interactions

(A and B) Proximity ligation assay for Ush1c and Ush1g in the anterior maculae of *grxcr1*$^{+/+}$ (A) and *grxcr1*$^{-/-}$ larvae (B) at 5 dpf.

(C) Quantification of Ush1c-Ush1g interactions in *grxcr1*$^{+/+}$ (n = 44 larvae), *grxcr1*$^{-/-}$ larvae (n = 45 larvae), and *grxcr1*$^{+/+}$ larvae that were incubated with only one primary antibody (control, n = 11 larvae). Data were normalized to *grxcr1*$^{+/+}$. Individual hair cells are outlined in white. Nuclei are outlined in blue.

(D) MDCK cells were transfected with *ush1c-HA*, *ush1ga-GFP*, and *grxcr1-HA* (+) or not (–). Extracted proteins were immunoprecipitated with an anti-GFP antibody and blotted using anti-Ush1c, anti-GFP, and anti-HA antibodies.

(E) Quantification of the Ush1c level in bound fractions in the presence or absence of Grxcr1 (n = 4 experiments). Data were normalized to input and are presented as a ratio amount of normalized Ush1c in the presence of Grxcr1 over the amount of normalized Ush1c in the absence of Grxcr1.

Data are represented as mean ± SEM. *p < 0.05.

epitope in exon 2 (Figure S6F) and recognizes Ush1ga but not Ush1gb (Figures S6I and S6J). We found that the level of Ush1g signal was unchanged in the mutants (Figures 6J–6L), indicating that the decrease in Ush1ga signal is due to inaccessibility of the epitope when Ush1ga binds to proteins via its SAM domain.

We then analyzed the physical proximity of Ush1c and Ush1g using an *in situ* proximity ligation assay (PLA) that we previously adapted to quantify USH1 protein-protein interactions in hair cells (Blanco-Sánchez et al., 2014). In WT animals, we found that, when both Ush1c and Ush1g antibodies (experimental condition) or only the anti-Ush1g antibody (control condition) were used in the assay, the PLA signals between Ush1c and Ush1g were not statistically different (Figures 7A and 7C). This suggested that, under normal conditions, Ush1c and Ush1g are not in close proximity in the cell body of hair cells and/or that they form fewer complexes than can be detected with this assay. In contrast, the Ush1c-Ush1g PLA signal was increased by 35% in the *grxcr1*$^{-/-}$ mutants (Figures 7A–7C). We also examined Ush1c and Ush1g interactions by immunoprecipitation. For this, MDCK cells were co-transfected with vectors encoding HA-tagged Ush1c and GFP-tagged Ush1ga with or without a vector encoding HA-tagged Grxcr1. Cell lysates were immunoprecipitated using an anti-GFP antibody and analyzed by immunoblot with Ush1c, GFP, and HA antibodies (Figure 7D). We observed an increase of 65% in the amount of Ush1c pulled down with Ush1ga when Grxcr1 was absent compared with when Grxcr1 was present (Figure 7E). This suggests that Grxcr1 activity reduces the number of Ush1c-Ush1ga complexes that form, consistent with results from the PLA (Figures 7A–7C). Together, these observations indicate that Grxcr1 promotes widening of the stereocilia by preventing physical interaction between Ush1c and Ush1g.

Loss of Grxcr1 Function Does Not Affect the Assembly of the Ush1c, Cdh23, and Myo7aa Tip Link Complex

Because Grxcr1 localizes in the ER, where Ush1c preassembles with Cdh23 and Myo7aa (Blanco-Sánchez et al., 2014), we investigated the effects of Grxcr1 loss of function on assembly of this tripartite complex. Our previous result showed that Ush1c accumulates in the cell bodies of hair cells in *grxcr1* mutants (Figures 6D–6F). However, Myo7aa and Cdh23 signal intensities were unchanged in *grxcr1*$^{-/-}$ mutants, and there was no obvious alteration in their localization (Figures S7A and S7B).

To assess the physical proximity of Ush1c, Cdh23, and Myo7aa, we used a PLA. We found no significant changes in any of the pairwise PLA signals (Figures S7C–S7E), indicating that Grxcr1 does not regulate assembly of the Ush1c, Myo7aa, and Cdh23 tip link complex. We previously showed that perturbation of assembly of this tip link complex affects the integrity of the ERGIC, induces cell death, and causes mechanosensory defects (Blanco-Sánchez et al., 2014). Consistent with the PLA results, the ERGIC appeared normal in *grxcr1* mutants, as indicated by the ERGIC marker Trappc3 (Figures S7F–S7H).

DISCUSSION

The proper development, morphogenesis, and structural integrity of the hair cell mechanoreceptor rely on interactions among USH1 proteins assembled into complexes (Cosgrove and Zallocchi, 2014; El-Amraoui and Petit, 2005; Pan and Zhang, 2012). Ush1c and Ush1g are scaffold proteins that serve as organizational hubs for these complexes. Previous studies showed that Ush1c and Ush1g can interact together and with other USH1 proteins via their PDZ and SAM domains (Adato et al., 2005; Boëda et al., 2002; Siemens et al., 2002; Weil et al., 2003; Wu et al., 2011; Yan et al., 2010). However, because each scaffold protein contains limited numbers of

protein-protein interaction domains, it is unlikely that all USH1 proteins interact with Ush1c and Ush1g at the same time. Thus, assembly of USH1 proteins into different complexes is most probably dynamically regulated. Here we show that deglutathionylation by Grxcr1 regulates the formation of USH1 protein complexes by destabilizing the interactions between Ush1c and Ush1g and that failure to deglutathionylate leads to defects in hair bundle morphology.

Widening of the hair bundle during normal development occurs by increasing the size of the stereocilia with greater numbers of actin filaments and by addition of new stereocilia (Tilney et al., 1992; Tilney and DeRosier, 1986). Elongation relies initially on extension of the stereocilia surrounding the kinocilium and then stereocilia further away (Tilney and DeRosier, 1986). This wave of extension gives the hair bundle its staircase shape. Previous work revealed a role for the MET machinery in actin polymerization and, thus, in hair bundle development and maintenance (Caberlotto et al., 2011a, 2011b). In *Ush1g* mouse mutants, the amplitude of the MET current is decreased, and loss of tip links prevents F-actin renewal, leading to regression of stereocilia from the shorter rows. Our zebrafish *grxcr1* mutants have thinner hair bundles. We show that Grxcr1 regulates the number of Ush1c-Ush1ga complexes via its deglutathionylation activity. By promoting interaction of Ush1c with Ush1g, Grxcr1 could hinder the formation of other Ush1 complexes that depend on Ush1c or Ush1g. Thus, maintenance of the tip links and, as a result, actin polymerization will be reduced, leading to thinner hair bundles. Consistent with this interpretation, mouse *Grxcr1* mutants form thinner inner and outer hair cell stereocilia (Erven et al., 2002; Odeh et al., 2010), suggesting a defect in actin polymerization.

Glutathionylation is a reversible posttranslational modification by addition of glutathione to a protein cysteine via a disulfide bond. In zebrafish, the transcript variant A of *ush1c* is the most abundant isoform (Phillips et al., 2011), and the encoded protein has a single cysteine located in the first PDZ domain (PDZ1). Structural analysis of the interaction between Ush1c PDZ1 and the SAM-PDZ binding motif (PBM) domain of USH1G revealed that this conserved cysteine localizes in the hydrophobic pocket of PDZ1, where the PBM domain of Ush1g binds (Yan et al., 2010). Colocalization of Ush1c and Ush1g is decreased when interactions between the USH1G PBM and Ush1c PDZ1 are weakened by mutations in these domains (Yan et al., 2010). Our finding that Ush1c and, possibly, Ush1ga are glutathionylated is consistent with this interaction model and further shows that glutathionylation dynamically regulates the stability of Ush1c and Ush1g interaction.

The roles of posttranslational modifications in the development of the mechanoreceptor remain understudied. Bauß et al. (2014) showed previously that Ush1g phosphorylation regulates Magi2-mediated endocytosis and that these two proteins can form a complex in the periciliary region of photoreceptors in the murine retina (Bauß et al., 2014). In *Drosophila*, the E3 ubiquitin ligase Ubr3 regulates development of the Johnston's auditory organ by negatively regulating MyoVIIa interaction with MyoII (Li et al., 2016). In humans, the Clrn1 USH protein is involved in regulation of the actin cytoskeleton (Tian et al., 2009), and a common missense mutation that substitutes a lysine for an asparagine leads to defective N-linked glycosylation of Clrn1, misfolding, and degradation by the proteasome (Tian et al., 2009). Our studies add to the importance of posttranslational modifications of USH proteins in hair cell development and function.

STAR★METHODS

Detailed methods are provided in the online version of this paper and include the following:

- KEY RESOURCES TABLE
- CONTACT FOR REAGENT AND RESOURCE SHARING
- EXPERIMENTAL MODEL AND SUBJECT DETAILS
  - Zebrafish
- METHOD DETAILS
  - Generation of indel mutant lines using CRISPR and TALEN
  - Immunolabeling and phalloidin staining
  - Proximity ligation assay
  - TUNEL labeling
  - Behavior assay
  - Co-immunoprecipitation and western blotting
  - RT-PCR
  - *in situ* hybridization and histology
  - Startle response test
  - FM1-43 incorporation
- QUANTIFICATION AND STATISTICAL ANALYSIS
  - Image analysis and quantification
  - Statistical analysis

SUPPLEMENTAL INFORMATION

Supplemental Information includes seven figures and can be found with this article online at https://doi.org/10.1016/j.celrep.2018.10.005.

ACKNOWLEDGMENTS

We thank Jennifer C. Michel, Poh Kheng Loi, Reiko Matsui, and Markus Bachschmid for technical assistance. This work was supported by grants from the NIH (DC004186, OD011195, and HD22486).

AUTHOR CONTRIBUTIONS

B.B.-S. and A.C. conceptualized the project and designed the experiments. B.B.-S. and A.C. performed immunohistochemistry and western blot experiments, image analysis and quantification, and statistical analysis. J.F. Jr. performed cell culture and immunoprecipitation experiments with support from P.J.W. S.S. performed behavior experiments with support from P.J.W. B.B.-S., A.C., J.B.P., J.W., and J.L.P. generated and maintained and performed initial phenotypical characterization of the zebrafish mutant lines. J.M.P. performed immunohistochemistry. B.B.-S., A.C., and M.W. wrote the manuscript. All authors reviewed and edited the manuscript.

DECLARATION OF INTERESTS

The authors declare no competing interests.

Received: May 18, 2018
Revised: August 11, 2018
Accepted: September 28, 2018
Published: October 30, 2018

REFERENCES

Adato, A., Michel, V., Kikkawa, Y., Reiners, J., Alagramam, K.N., Weil, D., Yonekawa, H., Wolfrum, U., El-Amraoui, A., and Petit, C. (2005). Interactions in the network of Usher syndrome type 1 proteins. Hum. Mol. Genet. *14*, 347–356.

Allocati, N., Masulli, M., Di Ilio, C., and Federici, L. (2018). Glutathione transferases: substrates, inhibitors and pro-drugs in cancer and neurodegenerative diseases. Oncogenesis *7*, 8.

Barr-Gillespie, P.G. (2015). Assembly of hair bundles, an amazing problem for cell biology. Mol. Biol. Cell *26*, 2727–2732.

Bauß, K., Knapp, B., Jores, P., Roepman, R., Kremer, H., Wijk, E.V., Märker, T., and Wolfrum, U. (2014). Phosphorylation of the Usher syndrome 1G protein SANS controls Magi2-mediated endocytosis. Hum. Mol. Genet. *23*, 3923–3942.

Beyer, L.A., Odeh, H., Probst, F.J., Lambert, E.H., Dolan, D.F., Camper, S.A., Kohrman, D.C., and Raphael, Y. (2000). Hair cells in the inner ear of the pirouette and shaker 2 mutant mice. J. Neurocytol. *29*, 227–240.

Blanco-Sánchez, B., Clément, A., Fierro, J., Jr., Washbourne, P., and Westerfield, M. (2014). Complexes of Usher proteins preassemble at the endoplasmic reticulum and are required for trafficking and ER homeostasis. Dis. Model. Mech. *7*, 547–559.

Board, P.G., and Menon, D. (2016). Structure, function and disease relevance of Omega-class glutathione transferases. Arch. Toxicol. *90*, 1049–1067.

Boëda, B., El-Amraoui, A., Bahloul, A., Goodyear, R., Daviet, L., Blanchard, S., Perfettini, I., Fath, K.R., Shorte, S., Reiners, J., et al. (2002). Myosin VIIa, harmonin and cadherin 23, three Usher I gene products that cooperate to shape the sensory hair cell bundle. EMBO J. *21*, 6689–6699.

Caberlotto, E., Michel, V., de Monvel, J.B., and Petit, C. (2011a). Coupling of the mechanotransduction machinery and F-actin polymerization in the cochlear hair bundles. Bioarchitecture *1*, 169–174.

Caberlotto, E., Michel, V., Foucher, I., Bahloul, A., Goodyear, R.J., Pepermans, E., Michalski, N., Perfettini, I., Alegria-Prévot, O., Chardenoux, S., et al. (2011b). Usher type 1G protein sans is a critical component of the tip-link complex, a structure controlling actin polymerization in stereocilia. Proc. Natl. Acad. Sci. USA *108*, 5825–5830.

Cosgrove, D., and Zallocchi, M. (2014). Usher protein functions in hair cells and photoreceptors. Int. J. Biochem. Cell Biol. *46*, 80–89.

Cotanche, D.A. (1987). Development of hair cell stereocilia in the avian cochlea. Hear. Res. *28*, 35–44.

Dror, A.A., and Avraham, K.B. (2009). Hearing loss: mechanisms revealed by genetics and cell biology. Annu. Rev. Genet. *43*, 411–437.

El-Amraoui, A., and Petit, C. (2005). Usher I syndrome: unravelling the mechanisms that underlie the cohesion of the growing hair bundle in inner ear sensory cells. J. Cell Sci. *118*, 4593–4603.

Ernest, S., Rauch, G.J., Haffter, P., Geisler, R., Petit, C., and Nicolson, T. (2000). Mariner is defective in myosin VIIA: a zebrafish model for human hereditary deafness. Hum. Mol. Genet. *9*, 2189–2196.

Erven, A., Skynner, M.J., Okumura, K., Takebayashi, S., Brown, S.D., Steel, K.P., and Allen, N.D. (2002). A novel stereocilia defect in sensory hair cells of the deaf mouse mutant Tasmanian devil. Eur. J. Neurosci. *16*, 1433–1441.

Johnson, K.R., Gagnon, L.H., Webb, L.S., Peters, L.L., Hawes, N.L., Chang, B., and Zheng, Q.Y. (2003). Mouse models of USH1C and DFNB18: phenotypic and molecular analyses of two new spontaneous mutations of the Ush1c gene. Hum. Mol. Genet. *12*, 3075–3086.

Johnson, W.M., Wilson-Delfosse, A.L., Chen, S.G., and Mieyal, J.J. (2015). The roles of redox enzymes in Parkinson's disease: Focus on glutaredoxin. Ther. Targets Neurol. Dis. *2*, e790.

Kimmel, C.B., Ballard, W.W., Kimmel, S.R., Ullmann, B., and Schilling, T.F. (1995). Stages of embryonic development of the zebrafish. Dev. Dyn. *203*, 253–310.

Lefèvre, G., Michel, V., Weil, D., Lepelletier, L., Bizard, E., Wolfrum, U., Hardelin, J.P., and Petit, C. (2008). A core cochlear phenotype in USH1 mouse mutants implicates fibrous links of the hair bundle in its cohesion, orientation and differential growth. Development *135*, 1427–1437.

Li, T., Giagtzoglou, N., Eberl, D.F., Jaiswal, S.N., Cai, T., Godt, D., Groves, A.K., and Bellen, H.J. (2016). The E3 ligase Ubr3 regulates Usher syndrome and MYH9 disorder proteins in the auditory organs of Drosophila and mammals. eLife *5*, e15258.

Lu, X., and Sipe, C.W. (2016). Developmental regulation of planar cell polarity and hair-bundle morphogenesis in auditory hair cells: lessons from human and mouse genetics. Wiley Interdiscip. Rev. Dev. Biol. *5*, 85–101.

Mathur, P., and Yang, J. (2015). Usher syndrome: Hearing loss, retinal degeneration and associated abnormalities. Biochim. Biophys. Acta *1852*, 406–420.

Matsui, R., Watanabe, Y., and Murdoch, C.E. (2017). Redox regulation of ischemic limb neovascularization - What we have learned from animal studies. Redox Biol. *12*, 1011–1019.

McGrath, J., Roy, P., and Perrin, B.J. (2017). Stereocilia morphogenesis and maintenance through regulation of actin stability. Semin. Cell Dev. Biol. *65*, 88–95.

Mori, K., Miyanohara, I., Moteki, H., Nishio, S.Y., Kurono, Y., and Usami, S. (2015). Novel mutation in GRXCR1 at DFNB25 lead to progressive hearing loss and dizziness. Ann. Otol. Rhinol. Laryngol. *124* (*Suppl 1*), 129S–134S.

Nicolson, T., Rüsch, A., Friedrich, R.W., Granato, M., Ruppersberg, J.P., and Nüsslein-Volhard, C. (1998). Genetic analysis of vertebrate sensory hair cell mechanosensation: the zebrafish circler mutants. Neuron *20*, 271–283.

Odeh, H., Hunker, K.L., Belyantseva, I.A., Azaiez, H., Avenarius, M.R., Zheng, L., Peters, L.M., Gagnon, L.H., Hagiwara, N., Skynner, M.J., et al. (2010). Mutations in Grxcr1 are the basis for inner ear dysfunction in the pirouette mouse. Am. J. Hum. Genet. *86*, 148–160.

Pan, L., and Zhang, M. (2012). Structures of usher syndrome 1 proteins and their complexes. Physiology (Bethesda) *27*, 25–42.

Pastore, A., and Piemonte, F. (2012). S-Glutathionylation signaling in cell biology: progress and prospects. Eur. J. Pharm. Sci. *46*, 279–292.

Petit, C., and Richardson, G.P. (2009). Linking genes underlying deafness to hair-bundle development and function. Nat. Neurosci. *12*, 703–710.

Phillips, J.B., Blanco-Sanchez, B., Lentz, J.J., Tallafuss, A., Khanobdee, K., Sampath, S., Jacobs, Z.G., Han, P.F., Mishra, M., Titus, T.A., et al. (2011). Harmonin (Ush1c) is required in zebrafish Müller glial cells for photoreceptor synaptic development and function. Dis. Model. Mech. *4*, 786–800.

Schraders, M., Lee, K., Oostrik, J., Huygen, P.L., Ali, G., Hoefsloot, L.H., Veltman, J.A., Cremers, F.P., Basit, S., Ansar, M., et al. (2010). Homozygosity mapping reveals mutations of GRXCR1 as a cause of autosomal-recessive nonsyndromic hearing impairment. Am. J. Hum. Genet. *86*, 138–147.

Seiler, C., Finger-Baier, K.C., Rinner, O., Makhankov, Y.V., Schwarz, H., Neuhauss, S.C., and Nicolson, T. (2005). Duplicated genes with split functions: independent roles of protocadherin15 orthologues in zebrafish hearing and vision. Development *132*, 615–623.

Shao, D., Fry, J.L., Han, J., Hou, X., Pimentel, D.R., Matsui, R., Cohen, R.A., and Bachschmid, M.M. (2014). A redox-resistant sirtuin-1 mutant protects against hepatic metabolic and oxidant stress. J. Biol. Chem. *289*, 7293–7306.

Siemens, J., Kazmierczak, P., Reynolds, A., Sticker, M., Littlewood-Evans, A., and Müller, U. (2002). The Usher syndrome proteins cadherin 23 and harmonin form a complex by means of PDZ-domain interactions. Proc. Natl. Acad. Sci. USA *99*, 14946–14951.

Söllner, C., Rauch, G.J., Siemens, J., Geisler, R., Schuster, S.C., Müller, U., and Nicolson, T.; Tübingen 2000 Screen Consortium (2004). Mutations in cadherin 23 affect tip links in zebrafish sensory hair cells. Nature *428*, 955–959.

Thisse, B., and Thisse, C. (2004). Fast Release Clones: A High Throughput Expression Analysis. ZFIN Direct Data Submission, ZDB-PUB-040907-1.

Tian, G., Zhou, Y., Hajkova, D., Miyagi, M., Dinculescu, A., Hauswirth, W.W., Palczewski, K., Geng, R., Alagramam, K.N., Isosomppi, J., et al. (2009). Clarin-1, encoded by the Usher Syndrome III causative gene, forms a

membranous microdomain: possible role of clarin-1 in organizing the actin cytoskeleton. J. Biol. Chem. *284*, 18980–18993.

Tilney, L.G., and DeRosier, D.J. (1986). Actin filaments, stereocilia, and hair cells of the bird cochlea. IV. How the actin filaments become organized in developing stereocilia and in the cuticular plate. Dev. Biol. *116*, 119–129.

Tilney, L.G., Tilney, M.S., Saunders, J.S., and DeRosier, D.J. (1986). Actin filaments, stereocilia, and hair cells of the bird cochlea. III. The development and differentiation of hair cells and stereocilia. Dev. Biol. *116*, 100–118.

Tilney, L.G., Cotanche, D.A., and Tilney, M.S. (1992). Actin filaments, stereocilia and hair cells of the bird cochlea. VI. How the number and arrangement of stereocilia are determined. Development *116*, 213–226.

Wang, L., Qu, G., Gao, Y., Su, L., Ye, Q., Jiang, F., Zhao, B., and Miao, J. (2018). A small molecule targeting glutathione activates Nrf2 and inhibits cancer cell growth through promoting Keap-1 S-glutathionylation and inducing apoptosis. RSC Advances *8*, 792–804.

Weil, D., El-Amraoui, A., Masmoudi, S., Mustapha, M., Kikkawa, Y., Lainé, S., Delmaghani, S., Adato, A., Nadifi, S., Zina, Z.B., et al. (2003). Usher syndrome type I G (USH1G) is caused by mutations in the gene encoding SANS, a protein that associates with the USH1C protein, harmonin. Hum. Mol. Genet. *12*, 463–471.

Westerfield, M. (2007). The Zebrafish Book. A Guide for the Laboratory Use of Zebrafish (Danio rerio) (Eugene, OR: University of Oregon Press).

Wu, L., Pan, L., Wei, Z., and Zhang, M. (2011). Structure of MyTH4-FERM domains in myosin VIIa tail bound to cargo. Science *331*, 757–760.

Yan, J., Pan, L., Chen, X., Wu, L., and Zhang, M. (2010). The structure of the harmonin/sans complex reveals an unexpected interaction mode of the two Usher syndrome proteins. Proc. Natl. Acad. Sci. USA *107*, 4040–4045.

Zerbino, D.R., Achuthan, P., Akanni, W., Amode, M.R., Barrell, D., Bhai, J., Billis, K., Cummins, C., Gall, A., Girón, C.G., et al. (2018). Ensembl 2018. Nucleic Acids Res. *46* (*D1*), D754–D761.

STAR★METHODS

KEY RESOURCES TABLE

REAGENT or RESOURCE	SOURCE	IDENTIFIER
Antibodies		
Rabbit polyclonal anti-GRXCR1	Novus Biologicals	Cat# NBP1-90591; RRID: AB_11028153
Mouse monoclonal anti-GM130	BD Biosciences	Cat# 610822; RRID: AB_398141
Mouse monoclonal anti-KDEL	Millipore	Cat# 420400-50UG; RRID: AB_212090
Rabbit polyclonal anti-USH1C	Novus Biologicals	Cat# 20920002; RRID: AB_11017833
Guinea pig polyclonal anti-USH1GA	This paper	N/A
Rabbit polyclonal anti-USH1G	Novus Biologicals	Cat# NBP1-89076; RRID: AB_11036031
Mouse monoclonal anti-USH1G	Santa Cruz Biotechnology	Cat# sc-514418
Goat polyclonal anti-USH1G	Santa Cruz Biotechnology	Cat# sc-69070
Rabbit polyclonal anti-TRAPPC3	Sigma Aldrich	Cat# SAB4501193; RRID: AB_10745271
Rabbit polyclonal anti-CDH23	Sigma Aldrich	Cat# HPA017232; RRID: AB_1845903
Goat polyclonal anti-cadherin-23	Santa Cruz Biotechnology	Cat# sc-26338; RRID: AB_634513
Mouse monoclonal anti-Myosin VIIa	Santa Cruz Biotechnology	Cat# sc-74516; RRID: AB_2148626
Chicken polyclonal anti-Myo7aa	Blanco-Sánchez et al., 2014	N/A
Rabbit polyclonal anti-GFP	Torrey Pines Biolabs	Cat# TP401 071519; RRID: AB_10013661
Mouse monoclonal anti-HA	Covance	Cat# MMS-101R
Mouse monoclonal anti-Glutathione	ViroGen	Cat# 101-A-100
Goat anti-mouse IgG, biotinylated	Vector Laboratories	Cat# BA-9200; RRID: AB_2336171
Goat anti-rabbit IgG, biotinylated	Vector Laboratories	Cat# BA-1100; RRID: AB_2336201
Horse anti-goat IgG, biotinylated	Vector Laboratories	Cat# BA-9500; RRID: AB_2336123
Goat anti-guinea pig IgG, biotinylated	Vector Laboratories	Cat# BA-7000; RRID: AB_2336132
Goat anti-chicken IgG, biotinylated	Vector Laboratories	Cat# BA-9010; RRID: AB_2336114
Goat anti-mouse, Alexa Fluor-568-conjugated	Molecular Probes	Cat# A-11004; RRID: AB_141371
Goat anti-rabbit, Alexa Fluor-488-conjugated	Molecular Probes	Cat# A-11008; RRID: AB_143165
Goat anti-guinea pig, Alexa Fluor-546-conjugated	Thermo Fisher Scientific	Cat# A-11074; RRID: AB_2534118
Cy3 AffiniPure Donkey Anti-Goat IgG	Jackson ImmunoResearch Labs	Cat# 705-165-147; RRID: AB_2307351
Sheep Anti-Digoxigenin Fab fragments Antibody, AP Conjugated	Roche	Cat# 11093274910; RRID: AB_514497
Alexa Fluor 488 Phalloidin	Thermo Fisher Scientific	Cat# A12379; RRID: AB_2315147
Chemicals, Peptides, and Recombinant Proteins		
MS-222 (tricaine-S)	Syndel USA	N/A
Vectashield mounting medium	Vector Laboratories	Cat# H-1000
nProtein A Sepharose 4 fast flow	GE Healthcare	Cat# 17-5280-01
FM1-43fx	Molecular probes	Cat# F35355
Critical Commercial Assays		
Lipofectamine 2000 Transfection Reagent	Thermo Fisher Scientific	Cat# 11668027
VECTASTAIN Elite ABC-HRP Kit	Vector Laboratories	Cat# PK-6100
Duolink *In Situ* Detection reagents green	Sigma Aldrich	Cat# DUO92014
ApopTag Peroxidase *In Situ* Apoptosis Detection kit	Millipore	Cat# S7100
Experimental Models: Cell Lines		
Canine: MDCK	ATCC	N/A
Experimental Models: Organisms/Strains		
Zebrafish: *grxcr1*^{b1259}	This paper	N/A
Zebrafish: *grxcr1*^{b1260}	This paper	N/A

(*Continued on next page*)

Continued

REAGENT or RESOURCE	SOURCE	IDENTIFIER
Zebrafish: *ush1c*^{fh293}	Phillips et al., 2011	N/A
Zebrafish: *ush1ga*^{b1240}	This paper	N/A
Zebrafish: *ush1ga*^{b1342}	This paper	N/A
Zebrafish: *Tg[myo6b:kdel-crimson]*^{b1319}	This paper	N/A
Oligonucleotides		
grxcr1-sgRNA1: GACACCTGTGCGGACTCCT	This paper	N/A
grxcr1-gF1: GTCAACGCAatggaggagtc	This paper	N/A
grxcr1-gR1: CCAACAATCTACATATAATTGACC	This paper	N/A
grxcr1-sgRNA2: GGAGACTCGCTGCAAACGAG	This paper	N/A
grxcr1-gF2: aattgactcttgagtttggccg	This paper	N/A
grxcr1-gR2: CAAATCAATAGAGGCTTGGACC	This paper	N/A
ush1ga-sgRNA: GGCCTTCCGGGATGCCGAA	This paper	N/A
ush1ga-gF2: GTCCTTCCTGGTGTCCTTTGG	This paper	N/A
ush1ga-gR2: CTGGGAGTATGGCACATTAGTGG	This paper	N/A
Recombinant DNA		
grxcr1-HA	This paper	N/A
ush1c-HA	Blanco-Sánchez et al., 2014	N/A
ush1ga-HA	This paper	N/A
ush1ga-GFP	This paper	N/A
ush1gb-HA	This paper	N/A
Software and Algorithms		
ImageJ 1.44o	NIH	RRID: SCR_003070
Prism 6	GraphPad	RRID: SCR_002798

CONTACT FOR REAGENT AND RESOURCE SHARING

Further information and requests for resources and reagents should be directed to and will be fulfilled by the Lead Contact, Bernardo Blanco Sanchez (berde@uoneuro.uoregon.edu).

EXPERIMENTAL MODEL AND SUBJECT DETAILS

Zebrafish

Homozygous wild-types (WT), *grxcr1*$^{+/+}$, homozygous mutants, *grxcr1*$^{b1259/b1259}$ and *grxcr1*$^{b1260/b1260}$, heterozygous mutants, *grxcr1*$^{b1259/+}$ (p.G67fsX132), *grxcr1*$^{b1260/+}$ (p.C201fsX203), *ush1c*$^{fh293/+}$ (p.L162X), *ush1ga*$^{b1240/+}$ (p.D15fsX21) and *ush1ga*$^{b1342/+}$ (p.144fsX151), *Tg[myo6b:kdel-crimson]*^{b1319}, and WT ABCxTu adult zebrafish were maintained as previously described (Westerfield, 2007). Embryos and larvae were staged according to the standard staging series (Kimmel et al., 1995). Siblings are defined as a mix of homozygous WT and heterozygous mutants generated by incrosses of heterozygous mutant adults. All experimental procedures were approved by the local IACUC.

Cell lines

MDCK cells were cultured in DMEM supplemented with 10% fetal bovine serum and penicillin (40 U/ml)/streptomycin (40 μg/ml) at 37°C under 5% CO_2. Cells were transfected with 1 μg of plasmid of interest using Lipofectamine 2000. For cells that were treated with the reducing agent dithiotreitol (DTT), 30 mM DTT was added to the cell medium for 1 hour at 37°C.

METHOD DETAILS

Generation of indel mutant lines using CRISPR and TALEN

For the mutant lines generated with CRISPR, two single guide RNAs (sgRNA) were designed that contained targeting sequences in exon 1 (5′-GACACCTGTGCGGACTCCT-3′) and exon 2 (5′-GGAGACTCGCTGCAAACGAG-3′) of *grxcr1*, and one sgRNA was designed that contained a targeting sequence in exon 2 (5′-GGCCTTCCGGGATGCCGAA-3′) of *ush1ga*. sgRNA and *cas9* RNAs were co-injected at the 1-cell stage.

For the mutant lines generated with TALEN, a TALEN target site was designed in exon 1 (5′-CGGGATGGCTACCTC[gacctgcttaaa gaagcg]ACGCGGAAGGACCTGA-3′, spacer is indicated in bracket) of *ush1ga*. TALEN mRNA was injected at the 1-cell stage.

Indels mutations were identified using the following primers: Targeted sequence in exon 1 of *grxcr1*: forward 5′-GTCAACGCAATG GAGGAGTC-3′ and reverse: 5′-CCAACAATCTACATATAATTGACC-3′; targeted sequence in exon 2 of *grxcr1*: forward: 5′-AATT GACTCTTGAGTTTGGCCG-3′ and reverse: 5′-CAAATCAATAGAGGCTTGGACC-3′; targeted sequence in exon 1 of *ush1ga*: forward 5′-CTCCAAACCTGATGCTCAGC-3′ and reverse: 5′-CTGGGTCTTACCCTCTCCCTG-3′; targeted sequence in exon 2 of *ush1ga*: forward: 5′-GTCCTTCCTGGTGTCCTTTGG-3′ and reverse: 5′-CTGGGAGTATGGCACATTAGTGG-3′.

Immunolabeling and phalloidin staining

Wholemount larvae labeling was performed following our published protocol (Blanco-Sánchez et al., 2014) with minor modifications. 5 dpf larvae were anesthetized with MS-222 (tricaine-S; Syndel USA) at 4 g/l, fixed in BT fix overnight and permeabilized in 2.5% tween-20 for 18 hours. For colocalization with ER markers, 15 min acetone crack was performed. For single and double immunolabeling, following a 2-hours blocking step (PBS + 0.01% Tween-20 + 5% bovine serum albumin + 5% goat serum), the larvae were incubated overnight at 4°C with primary antibodies. Primary antibodies were rabbit anti-Grxcr1 (Novus Biologicals, 1:500), mouse anti-Gm130 (BD Transduction Laboratories, 1:500), mouse anti-KDEL (Calbiochem, 1:500), rabbit anti-Harmonin (Ush1c, Novus Biologicals, 1:500), guinea pig anti-Ush1ga (custom made against C-terminal region, 1-500), rabbit anti-Ush1g (Novus Biologicals, 1:500), mouse anti-Ush1g (Santa Cruz Biotechnology, 1:500), goat anti-Ush1g (Santa Cruz Biotechnology, 1:500), rabbit anti-Trappc3 (Sigma, 1:500), rabbit anti-Cdh23 (Sigma, 1:500), chicken anti-Myo7aa (custom made against N-terminal region, 1:500). Larvae were then washed with four washes in PBST to remove unbound antibodies, blocked for two hours and incubated overnight at 4°C with secondary antibodies. Secondary antibodies were biotinylated horse anti-mouse, biotinylated horse anti-rabbit (Vector Laboratories, 1:500), biotinylated horse anti-guinea pig, biotinylated horse anti-goat, biotinylated horse anti-chicken (Vector Laboratories, 1:250). Detection was done using the Vectastain ABC Elite kit (Vector laboratories) and stopped in PBST. For double immunolabeling, larvae were post-fixed for 20 minutes in BT fix and washed in PBST. The horse radish peroxidase (HRP) was quenched using 0.1 M HCl. After 2-hours block, the samples were incubated overnight at 4°C with secondary antibodies. Detection was done as described above.

Phalloidin staining procedure followed similar steps as the wholemount larvae labeling described here, but phalloidin was added instead of primary antibodies.

For cell-culture labeling, cells were fixed in BT fix for 10 minutes and permeabilized with 0.25% Triton X-100 in PBS. Detection was performed using rabbit anti-Grxcr1 (Novus Biologicals, 1:250), mouse anti-HA (Covance, 1:250), guinea pig anti-Ush1ga (Custom made against C-terminal region, 1:250), rabbit anti-Ush1g (Novus Biologicals, 1:500), mouse anti-Ush1g (Santa Cruz Biotechnology, 1:500), goat anti-Ush1g (Santa Cruz Biotechnology, 1:500), rabbit anti-GFP (Torrey Pines Biolabs, 1:250) antibodies. Secondary antibodies were goat anti-mouse Alexa Fluor-568-conjugated, goat anti-rabbit Alexa Fluor-488-conjugated, goat anti-guinea pig Alexa Fluor-568-conjugated, horse anti-goat Alexa Fluor-568-conjugated (Molecular probes, 1:250).

Images of immunolabeled larvae and cells were acquired using a Zeiss LSM 5 confocal microscope.

Proximity ligation assay

The larvae were prepared as described in the previous section. Primary antibodies were rabbit anti-Harmonin (Ush1c, Novus Biologicals), rabbit anti-Ush1g (Novus Biologicals, 1:500), mouse anti-Ush1g (Santa Cruz Biotechnology), goat anti-Ush1g (Santa Cruz Biotechnology), Rabbit anti-Cdh23 (Sigma), goat anti-Cdh23 (Santa Cruz Biotechnology), mouse anti-Myo7a (Santa Cruz Biotechnology). All primary antibodies were used at 1:500. After washing off the primary antibodies in PBST, the larvae were incubated 1 hour at 37°C in PBST, incubated for 4 hours at 37°C with the Duo-Link ligation solution (Olink Bioscience) and then overnight in Duo-Link amplification solution (Olink Bioscience).

Images of immunolabeled larvae were acquired using a Zeiss LSM 5 confocal microscope.

TUNEL labeling

Apoptag plus Peroxidase *In situ* Apoptosis Detection Kit was used. 5 dpf larvae were anesthetized with MS-222, fixed in BT fix overnight and stored overnight in 100% Methanol. After rehydration, the larvae were permeabilized for 1 hour in Proteinase K (1 μg/ml), post-fixed for 20 minutes in BT fix and incubated in acetone/ethanol mix (1:2) for 15 minutes at −20°C. The samples were equilibrated for 1 hour at room temperature in equilibration buffer, incubated for 90 minutes at 37°C in reaction solution (16 μL TdT enzyme + 38 μL reaction buffer). The reaction was stopped by addition of 200 μL stop buffer overnight at 37°C. The samples were blocked for 2 hours and incubated overnight at 4°C with an anti-DIG coupled to HRP. After several washes in PBST, the reaction product was detected with DAB as a substrate.

Behavior assay

5 dpf larvae were placed individually into polystyrene tissue culture flasks containing 50 mL embryo medium and recorded at 6 Hz for 5 min using a Mightex BCN-B050-U camera at a resolution of 1296x972 pixels. Images were background subtracted and the particle analysis feature in ImageJ was used to obtain the position of the larvae in the flask at each time point. 20 zebrafish from each genotype (*grxcr1*$^{b1259-/-}$, *grxcr1*$^{b1259+/+}$, *grxcr1*$^{b1260-/-}$, and *grxcr1*$^{b1260+/+}$) were tested. Larvae that were immobile for greater

than 90% of the test period were excluded from statistical analysis (5 *grxcr1*$^{b1259+/+}$, 6 *grxcr1*$^{b1259-/-}$, 2 *grxcr1*$^{b1260+/+}$, and 3 *grxcr1*$^{b1260-/-}$ mutant larvae).

Co-immunoprecipitation and western blotting

Cells were lysed in 125 μl RIPA buffer for 20 minutes at 4°C. Proteins were extracted as previously described (Blanco-Sánchez et al., 2014). After centrifugation at 5000 rpm for 5 minutes, the supernatant was incubated overnight at 4°C with either mouse anti-GSH (Virogen), rabbit anti-Ush1c (Novus Biologicals) or rabbit anti-GFP (Torrey Pines Biolabs). Proteins were precipitated with protein A-Sepharose beads, washed in lysis buffer and eluted in lysis buffer and non-reducing sample buffer (1:1). The eluted proteins were separated by SDS-polyacrylamide gel electrophoresis and transferred to PVDF membranes. Detection was performed using rabbit anti-Harmonin (Ush1c, Novus Biologicals, 1:600), mouse anti-HA (Covance, 1:500), rabbit anti-GFP (Torrey Pines Biolabs, 1:250), and mouse anti-GSH (Virogen, 1:500) antibodies and the Odyssey Western Blotting Kit I LT (LI-COR) following the manufacturer recommendations.

RT-PCR

RNA was extracted from 0.75 and 3 hpf and 1, 2, 3, 4 and 5 dpf. PCR was performed after retro-transcription using the SuperScript® III First-Strand Synthesis System. Primers used were: *grxcr1* forward: 5′-AATTGACTCTTGAGTTTGGCCG-3′, *grxcr1* reverse: 5′-TTAGTGAGAACAGCTGGAGCA-3′, ef1rt forward: 5′-GCCCCTGCCAATGTAACCAC-3′, ef1rt reverse: 5′-TGCCAGG GACCATCTCAACAA-3′.

in situ hybridization and histology

The procedure followed previously published protocol (Thisse and Thisse, 2004). Larvae were hybridized with a digoxigenin labeled RNA probe spanning the whole coding sequence of *grxcr1*. Stained larvae were embedded in 1% agarose, 0.5% agar, 5% sucrose medium and 16 μm cryosections were cut. Images of larvae stained by *in situ* hybridization were acquired using a Zeiss Axioplan2 compound microscope.

Startle response test

The startle test was performed at 5 dpf by taping on the Petri dish containing the tested larvae (Phillips et al., 2011). Larvae swimming away from the tap were scored as wild-types. Larvae that did not respond, circled or reacted to the tap but did not swim away were scored as larvae with balance defects.

FM1-43 incorporation

Larvae were incubated for 3.5 minutes (inner ear hair cells) or 30 secondes (neuromast hair cells) in 3 μM FM1-43fx (Molecular probes). They were then rinsed in embryo medium, fixed in BT fix overnight and stored in vectashield.

QUANTIFICATION AND STATISTICAL ANALYSIS

Image analysis and quantification

Images were all analyzed using ImageJ. Quantification of hair bundles and hair cells, hair bundle length and width measurements and signal intensity quantification were all performed using ImageJ.

The intensity of the immunoblot signals was measured using ImageJ and normalized.

Statistical analysis

Each experiment was repeated at least three times. The number of larvae, cells or experiments used are reported in the figures.

For all statistical analysis, a Student's t test was performed. Standard error of the mean (SEM) and significance are indicated in the figures.